U.S. DEPARTMENT OF ENERGY | Office of Science

DOE/SC-ARM-TR-224

Aerosol and Cloud Optical Properties from the ARM Raman Lidars: The Feature Detection and Extinction (RLPROF-FEX) Value-Added Product

D Chand
T Thorsen
C Sivaraman
J Shilling
R Newsom
E Cromwell
C Flynn
J Comstock

August 2022

ARM

DISCLAIMER

DOE/SC-ARM-TR-224

Aerosol and Cloud Optical Properties from the ARM Raman Lidars: The Feature Detection and Extinction (RLPROF-FEX) Value-Added Product

D Chand, Pacific Northwest National Laboratory (PNNL)
R Newsom, PNNL
T Thorsen, National Aeronautics and Space Administration
E Cromwell, PNNL
C Sivaraman, PNNL
C Flynn, PNNL, University of Oklahoma
J Shilling, PNNL
J Comstock, PNNL

August 2022

Work supported by the U.S. Department of Energy,
Office of Science, Office of Biological and Environmental Research

Acronyms and Abbreviations

ADC	ARM Data Center
AERONET	Aerosol Robotic Network
AMF	ARM Mobile Facility
AOD	aerosol optical depth
ARM	Atmospheric Radiation Measurement
DOE	U.S. Department of Energy
ENA	Eastern North Atlantic
FEX	Feature Detection and Extinction
FOV	field of view
IPCC	Intergovernmental Panel on Climate Change
MODIS	Moderate Resolution Imaging Spectroradiometer
netCDF	Network Common Data Form
NFOV	narrow field of view
OLI	Oliktok Point
PI	principal investigator
PNNL	Pacific Northwest National Laboratory
QC	quality control
RL	Raman lidar
SGP	Southern Great Plains
VAP	value-added product
WFOV	wide field of view

Contents

Figures

Tables

1.0 General Description

Aerosols and their interactions and influence on clouds are among the main sources of uncertainties in radiative direct and indirect forcing (IPCC 2013). Continuous height-resolved measurements of cloud and aerosol optical properties are needed to reduce these uncertainties. Here we describe the Raman Lidar Profiles – Feature detection and Extinction (RLPROF-FEX) Value-Added Product (VAP) derived using Raman lidar data at multiple U.S. Department of Energy (DOE) Atmospheric Radiation Measurement (ARM) user facility sites. RLPROF-FEX provides estimates of extinction, backscatter, and depolarization using the algorithm described by Thorsen et al. 2015 and Thorsen and Fu 2015. This document provides a description of the FEX algorithm, its input and output data, and related details about the Raman lidar (RL) system.

2.0 The Raman Lidar System

The DOE ARM facility currently operates Raman lidars at the Southern Great Plains observatory (SGP), the Eastern North Atlantic observatory (ENA), and formerly with the third ARM Mobile Facility (AMF3) at Oliktok Point (OLI), Alaska. All of these RL systems incorporate nearly identical designs. Cloud and aerosol optical properties are estimated using return signals from elastic backscatter at 355 nm, and Raman-shifted backscatter due to atmospheric nitrogen at 387 nm. The RL system uses a 61 cm telescope and two fields of view. The wide field of view (WFOV) detection channels are optimized for measurement at lower altitudes and the narrow field of view (NFOV) channels are optimized for observations at higher altitudes. Additional specifications for the systems are listed in Table 1. More details about the RL system design and measurement capabilities are provided by Goldsmith et al. 1998, Turner et al. 2002, Newsom et al. 2009, Newsom et al. 2012, Newsom et al. 2013, and Turner et al. 2016.

Table 1. The RL system detail showing transmitter and receiver.

	Laser	Nd:YAG, Third harmonic
Transmitter	Transmitter wavelength	355 nm
	Pulse energy	300 mJ
	Pulse repetition frequency	30 Hz
	Pulse width	5 ns
Receiver	Telescope diameter	61 cm
	FOV	2 mrad (WFOV), 0.3 mrad (NFOV)
	Range resolution	7.5 m
	Pulse integration time	10 sec
	Data acquisition	simultaneous photon counting and analog voltage measurement
	Detectors	PMTs, Electron Tube 9954B

	Detection channels	Unpolarized WFOV elastic @ 355 nm Co-polarized NFOV elastic @ 355 nm Cross-polarized NFOV elastic at 355 nm WFOV Nitrogen @ 387 nm NFOV Nitrogen @ 387 nm

Key Points:

- The detection channels shown in the table above include only those channels that are used by the FEX algorithm.
- NFOV measurements provide better sensitivity because the solar background is lower, but the NFOV signal are strongly impacted by incomplete overlap between the transmitted laser beam and the receiver's FOV below about 4 km. The WFOV channels achieve complete overlap at a much lower altitude (~800 m) but are also much more sensitive to solar radiation.

3.0 Input Datastreams and Fields

The FEX algorithm requires the following inputs:

- RL MERGE data (rlprofmerge2news.c0)
- Radiosonde data (sondewnpn.b1)
- Configuration data (rllog.a0).

The MERGE algorithm represents the first level of processing of the raw RL data. This includes dead- time correction and the merging of the raw photon counting and analog voltage signals through a process known as "gluing" (Whiteman et al. 2006, Newsom et al. 2009, Newsom 2012). The FEX algorithm uses the output from the MERGE algorithm, i.e., the MERGE VAP, as well as radiosonde data from a co-located launch site. The third set of inputs include various constants and corrections that are stored in configuration files. These include empirically derived estimates of the Angstrom exponent, aerosol effective size, depolarization misalignment angle, cloud droplet effective size, and overlap functions. The Angstrom exponent, aerosol effective size, and cloud droplet effective size are estimated from Aerosol Robotic Network (AERONET), and Moderate Resolution Imaging Spectroradiometer (MODIS) satellite data. Overlap functions and the depolarization misalignment angle are estimated from the raw RL data. Additional detail on how these inputs are used is discussed in Algorithm and Methodology, section 4.0.

Key points:

- Input data sources include the MERGE VAP, collocated radiosonde data, and configuration files.
- Configuration files provide site-specific default values for overlap functions, Angstrom exponents, aerosol size, depolarization misalignment angle, and cloud droplet size.
- Parameters in configuration files are estimated from long-term averages.

4.0 Algorithm and Methodology

Details of the FEX algorithm are given in Thorsen et al. (2015) and Thorsen and Fu (2015). This section provides a brief overview.

As indicated in Table 1, the FEX algorithm makes use of the polarized and unpolarized elastic return signals, as well as the Raman-shifted return signals from atmospheric nitrogen (at 387 nm). The symbols "e" and "N2" are used for elastic and Raman-scattered signal from nitrogen molecules, respectively, throughout this document. During the initial processing phase, the FEX algorithm computes the following quantities

a) Scattering ratio derived using the NFOV and WFOV elastic and nitrogen channel signals.

b) Scattering ratio derived using the measured NFOV and WFOV elastic channels, and modeled nitrogen signals.

c) Total volume depolarization ratio from the NFOV co- and cross-polarization elastic channels.

As explained in Thorsen et al (2015), the FEX algorithm computes the scattering ratio using two different methods, i.e., with and without the observed nitrogen signal. Range-dependent detection thresholds are applied to the scattering and depolarization ratios to identify features such as aerosol, cloud (liquid versus ice), and precipitation. Consistency checks are applied to features detected from the various ratios to obtain the best possible feature mask. Typically, inputs from 2-5 days prior are used to initiate the data processing to provide output for a desired period. For example, if we need the FEX output for January 15, the process will feed the input data from January 13 and start processing until January 15. A process starting a few days in advance can develop some background information on the calibration constant and overlap functions so that it can give the best results for the desired day.

A flow diagram for feature mask is shown in Figure 1. The FEX algorithm uses an iterative approach in which refinements are made to the scattering ratios, feature mask, depolarization ratio, backscatter, and extinction coefficients until the algorithm converges to a desired solution. During each iteration, the overlap functions, calibration constants, and detection limits are adjusted, and consistency checks are applied to reduce false detections. Convergence (desired solution) is achieved when the difference in the feature mask (from one iteration to the next) falls below a prescribed threshold. In the end, the FEX algorithm reports best estimates of the particulate extinction coefficient (corrected for multiple scattering effects), volume backscatter coefficient, lidar ratio, scattering ratio, and depolarization ratio, as well as more than 100 additional fields related to system checks and information on FEX's processing decisions.

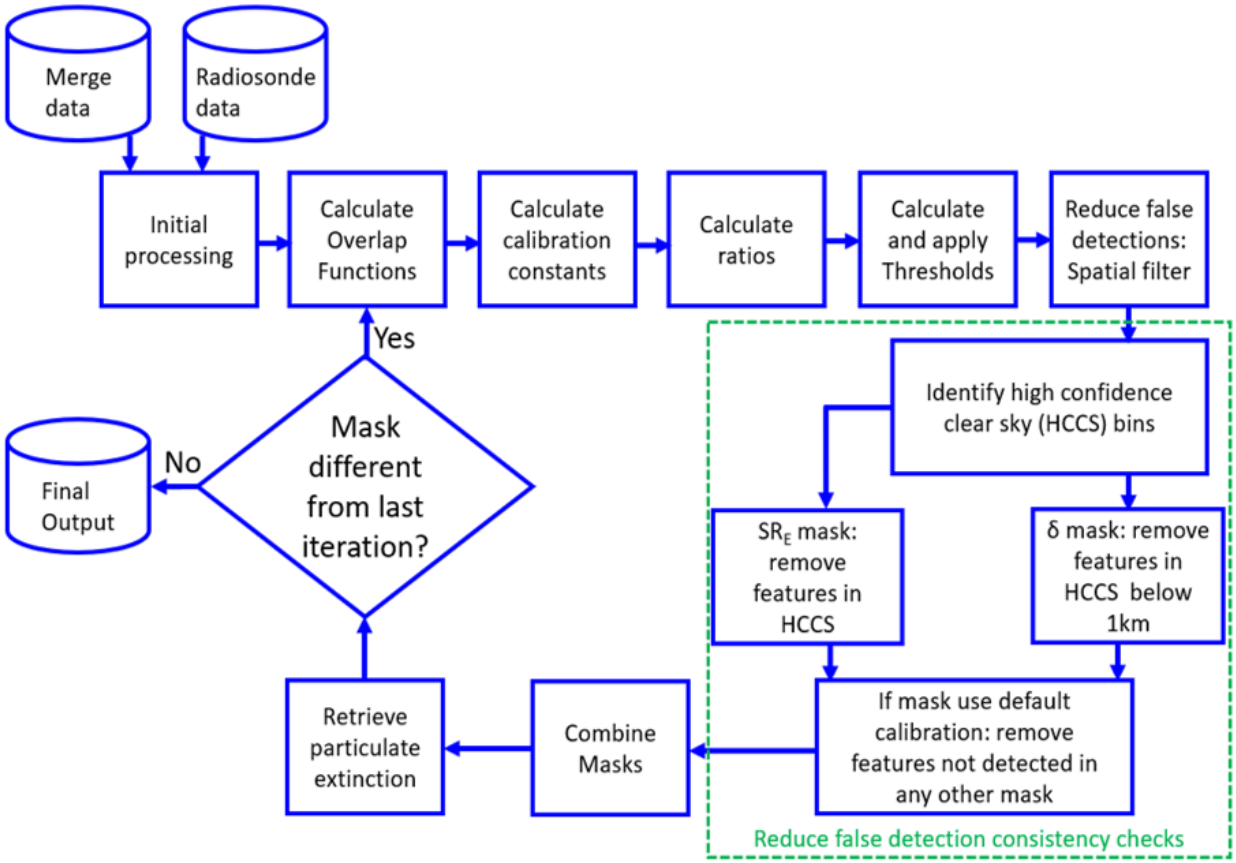

Figure 1. Flow diagram of feature detection and extinction (FEX) algorithm (Thorsen et al. 2015).

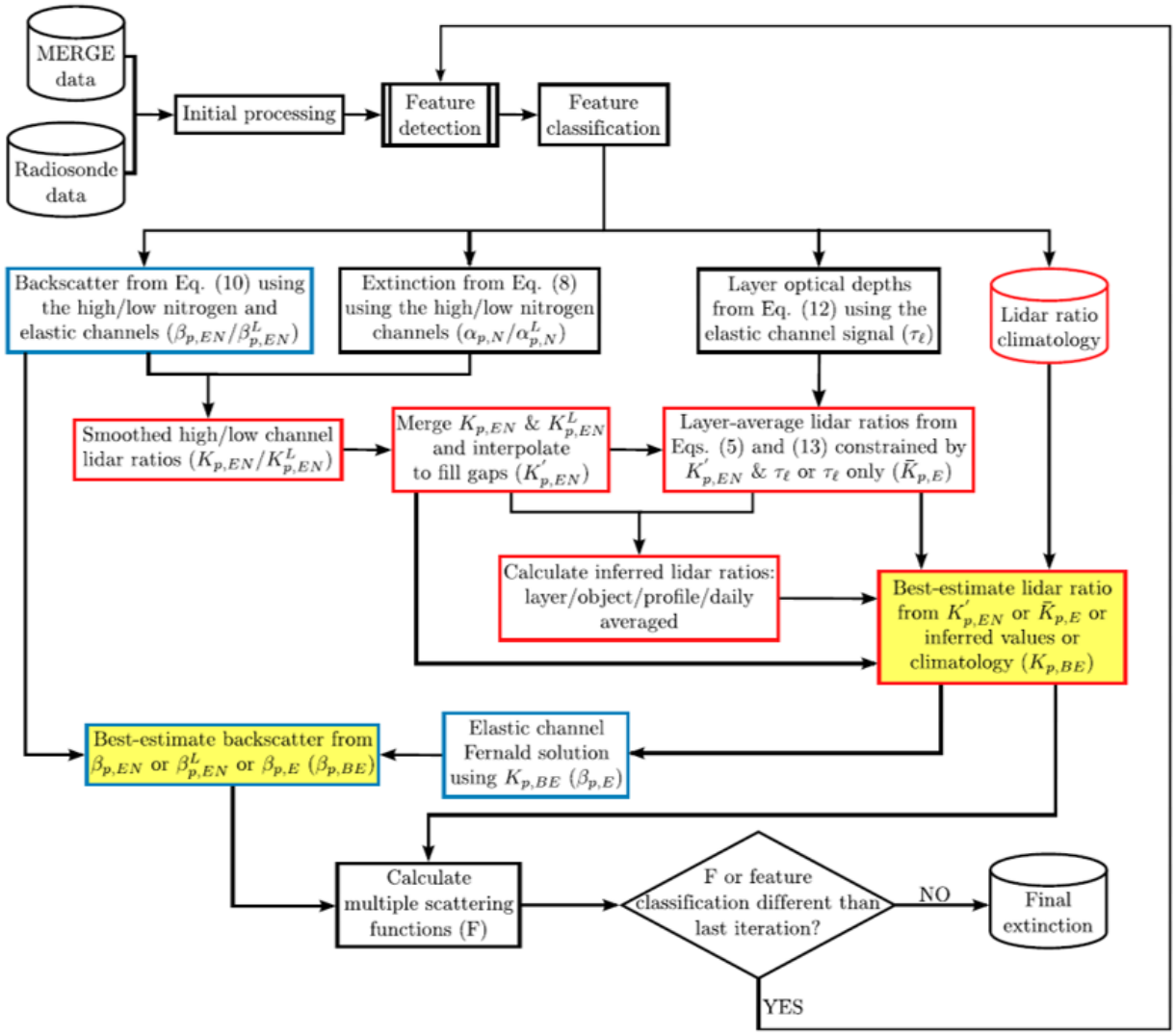

Figure 2. Flow diagram to estimate particulate extinction at 355 nm and feature classification. Blue and red boxes denote the retrievals of particulate backscatter coefficient and lidar ration, respectively. The best-estimate calculations occur in boxes with yellow backgrounds. The flow boxes and all the equations in this diagram are taken from Thorsen and Fu 2015.

5.0 FEX Output

The output of the FEX algorithm, i.e., the FEX VAP, consists of the following four separate datastreams:

1. rlproffex1thor.c0
2. rlproffexext1thor.c0
3. rlproffexaux1thor.c0
4. rlproffexcnt1thor.c0.

Of primary interest to the end user is the first datastream (rlproffex1thor.c0). This datastream contains the feature masks and best estimates of particulate extinction, backscatter, lidar ratio, and a number of other parameters. A complete listing of the primary variables in rlproffex1thor.c0 datastream is provided in Table 2. The remaining datastreams listed above contain intermediate results, calibration parameters, and raw photon-counting data. These results are primarily used by instrument mentors and operators to assess instrument performance. Listings of these datastream contents are provided in Appendix A. Subsections A.1-A.3 show details of a selection of features and related outputs.

Table 2. The primary fields in the reproffex1thor.c0 datastream.

Variable Name	Description
height_high(height_high)	Height above ground level for the high (NFOV) channels;
height_low(height_low)	Height above ground level for the low (WFOV) channels;
feature_mask(time, height_high)	Feature mask;
source_feature_mask(time, height_high)	Source for field: Feature mask;
extinction_flag(time, height_high)	Bit-wise flag that gives the detailed processing choices used for extinction;
detection_confidence_score_total(time, height_high)	Score indicating the confidence in the presence of a feature or clear-sky calculated using the estimated total uncertainty;
detection_confidence_score_random(time, height_high)	Score indicating the confidence in the presence of a feature or clear-sky calculated using only the random uncertainty;
pressure(time, height_high)	Pressure from radiosonde;
temperature(time, height_high)	Temperature from radiosonde;
wet_bulb_temperature(time, height_high)	Wet bulb temperature from radiosonde relative humidity and temperature;
scattering_ratio_e_n2(time, height_high)	Scattering ratio derived from the high elastic and nitrogen channels;
scattering_ratio_e_n2_uncertainty_random(time, height_high)	Random uncertainty in scattering_ratio_e_n2;
scattering_ratio_e_n2_uncertainty_systematic(time, height_high)	Systematic uncertainty in scattering_ratio_e_n2;
depolarization_ratio(time, height_high)	Volume linear depolarization ratio;
depolarization_ratio_uncertainty_random(time, height_high)	Random uncertainty in depolarization_ratio;
depolarization_ratio_uncertainty_systematic(time, height_high)	Systematic uncertainty in depolarization_ratio;

Variable Name	Description
scattering_ratio_e(time, height_high)	Scattering ratio derived from the high elastic channels;
scattering_ratio_e_uncertainty_random(time, height_high)	Random uncertainty in scattering_ratio_e;
scattering_ratio_e_uncertainty_systematic(time, height_high)	Systematic uncertainty in scattering_ratio_e;
scattering_ratio_e_n2_low(time, height_low)	Scattering ratio derived from the low elastic and nitrogen channels;
scattering_ratio_e_n2_low_uncertainty_random(time, height_low)	Random uncertainty in scattering_ratio_e_n2_low;
scattering_ratio_e_n2_low_uncertainty_systematic(time, height_low)	Maximum systematic uncertainty in scattering_ratio_e_n2_low;
particulate_backscatter_be(time, height_high)	Best-estimate of the particulate backscatter coefficient;
particulate_backscatter_be_uncertainty_random(time, height_high)	Random uncertainty in particulate_backscatter_be;
source_particulate_backscatter_be(time, height_high)	Source for field: Best-estimate of the particulate backscatter coefficient;
particulate_backscatter_be_uncertainty_systematic(time, height_high)	Maximum systematic uncertainty in particulate_backscatter_be;
lidar_ratio_be(time, height_high)	Best-estimate of the lidar ratio;
source_lidar_ratio_be(time, height_high)	Source for field: Best-estimate of the lidar ratio;
lidar_ratio_be_uncertainty_random(time, height_high)	Random uncertainty in lidar_ratio_be;
lidar_ratio_be_uncertainty_systematic(time, height_high)	Maximum systematic uncertainty in lidar_ratio_be;
extinction_be(time, height_high)	Best-estimate of the particulate extinction coefficient;
extinction_be_uncertainty_random(time, height_high)	Random uncertainty in extinction_be;
extinction_be_uncertainty_systematic(time, height_high)	Maximum systematic uncertainty in extinction_be;

5.1 Feature Mask

A key variable in the rlproffex1thor.c0 datastream is the feature mask (i.e., the “feature_mask” variable in Table 2). The feature mask is a bit-packed field in which various bits are used to indicate the presence of aerosol, clouds (liquid versus ice), and precipitation. If no bits are set, i.e., if the feature mask is 0, then no feature is detected, and the sample is deemed invalid. The various feature mask bits are:

bit_1 = feature (any type)
bit_2 = aerosol
bit_3 = cloud (any phase)
bit_4 = rain or virga
bit_5 = liquid cloud

bit_6 = ice cloud (any orientation)
bit_7 = horizontally oriented ice

5.2 Source Mask

The source mask (i.e., the "source_feature_mask" variable in Table 2) identifies the source variable that the feature was detected with. A value of 0 (no bits set) indicates no source. The source mask bits are defined as follows:

bit_1 = Feature detected in scattering_ratio_e_n2
bit_2 = Feature detected in scattering_ratio_e
bit_3 = Feature detected in depolarization ratio
bit_4 = Feature detected in scattering_ratio_e_n2_low

5.3 Sources of the Particulate Backscatter Best Estimate

The "source_particulate_backscatter_be" variable in Table 2 indicates the source of the backscatter best estimate. This variable can take on one of three values (1, 2, 4). The meanings of these values are described in Table 3.

Table 3. Possible values for the "source_particulate_backscatter_be" variable and their meanings.

Value	Meaning
1	WFOV backscatter using Raman method (particulate_backscatter_e_n2_low)
2	NFOV backscatter using Raman method (particulate_backscatter_e_n2)
4	Fernand solution using elastic signal (particulate_backscatter_e_beS)

5.4 Source of Lidar Ratio

The "source_lidar_ratio_be" in Table 2 indicates the source of lidar ratio best estimate. This variable can take on one of 10 values (1, 2, 4, 8, 16, 32, 64, 128, 256, 512). The meanings of these values are described in Table 4.

Table 4. Possible values for the "source_lidar_ratio_be" variable and their meanings.

Value	Meaning
1	WFOV lidar ratio (lidar_ratio_e_n2_low)
2	NFOV lidar ratio (lidar_ratio_e_n2)
4	Interpolated value
8	Fernald solution constrained by the sum of the low elastic channel lidar ratio, the high elastic channel lidar ratio, the interpolated solution, and the transmission-loss
16	Fernald solution constrained by the transmission-loss
32	Layer-averaged

64	Object-averaged
128	Profile-averaged
256	Daily-averaged
512	Prescribed

5.5 Detection Confidence Score

The “detection_confidence_score_total” variable in Table 2 indicates the confidence in the presence of a feature or clear sky calculated using the estimated total uncertainty. Score varies from 0 to 1. Values approaching 0 indicate the bin is more likely clear sky. Values approaching 1 indicate the bin is more likely a feature. A value of -1 is assigned where the laser beam is completely attenuated.

6.0 Data Quality Assessment

Estimates of random and systematic uncertainty are provided for all of the primary variables in the rlproffex1thor.c0 datastream. The random uncertainties in the final outputs are estimated from random noise in the raw lidar signals using standard error-propagation techniques. Sources of random uncertainty include (a) background noise due to solar radiation, detector dark current, thermal noise, and (b) shot noise. The systematic uncertainties are estimated from errors in calibration constants, overlap corrections, and the other constants defined in the configuration files. Figure 3 provides an example of the best- estimate extinction and its uncertainties for the SGP RL on June 1, 2019. This figure shows results with total confidence score of 0.3 or higher. In addition to the uncertainties, the confidence scores and/or feature mask can be used to screen the invalid data. The feature detection uncertainty is provided in the variables ‘detection_confidence_score_random’ and ‘detection_confidence_score_total’. The two values indicate the confidence in the presence of a feature or clear sky calculated using random or total uncertainty. The score varies from 0 to 1. Values approaching 0 indicate the bin is more likely clear sky, and 1 indicate the bin is more likely a feature. More details concerning the estimation of random and systematic uncertainty are provided in Thorsen et al. 2015 and Thorsen and Fu 2015.

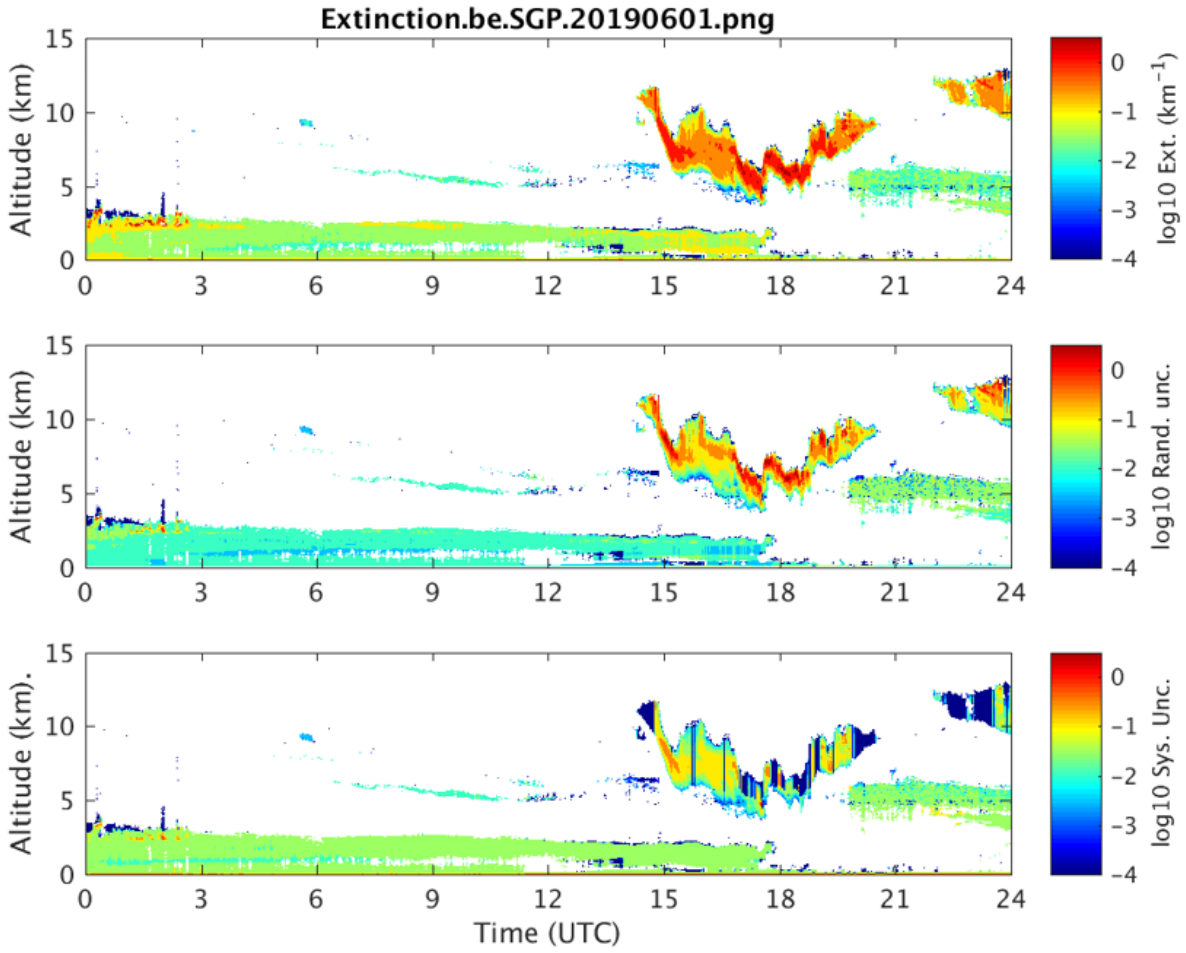

Figure 3. FEX-estimated value of particulate extinction (top panel) and its random (middle panel) and systematic (bottom panel) uncertainties on June 1, 2019 at SGP. Total confidence score of 0.3 or higher is used in this plot.

7.0 Data Plots

Figures 4 through 9 show some examples of FEX output variables that are of primary interest to end users. This includes the feature and source masks, particular extinction, backscatter, depolarization ratio, lidar ratio, and scattering ratio.

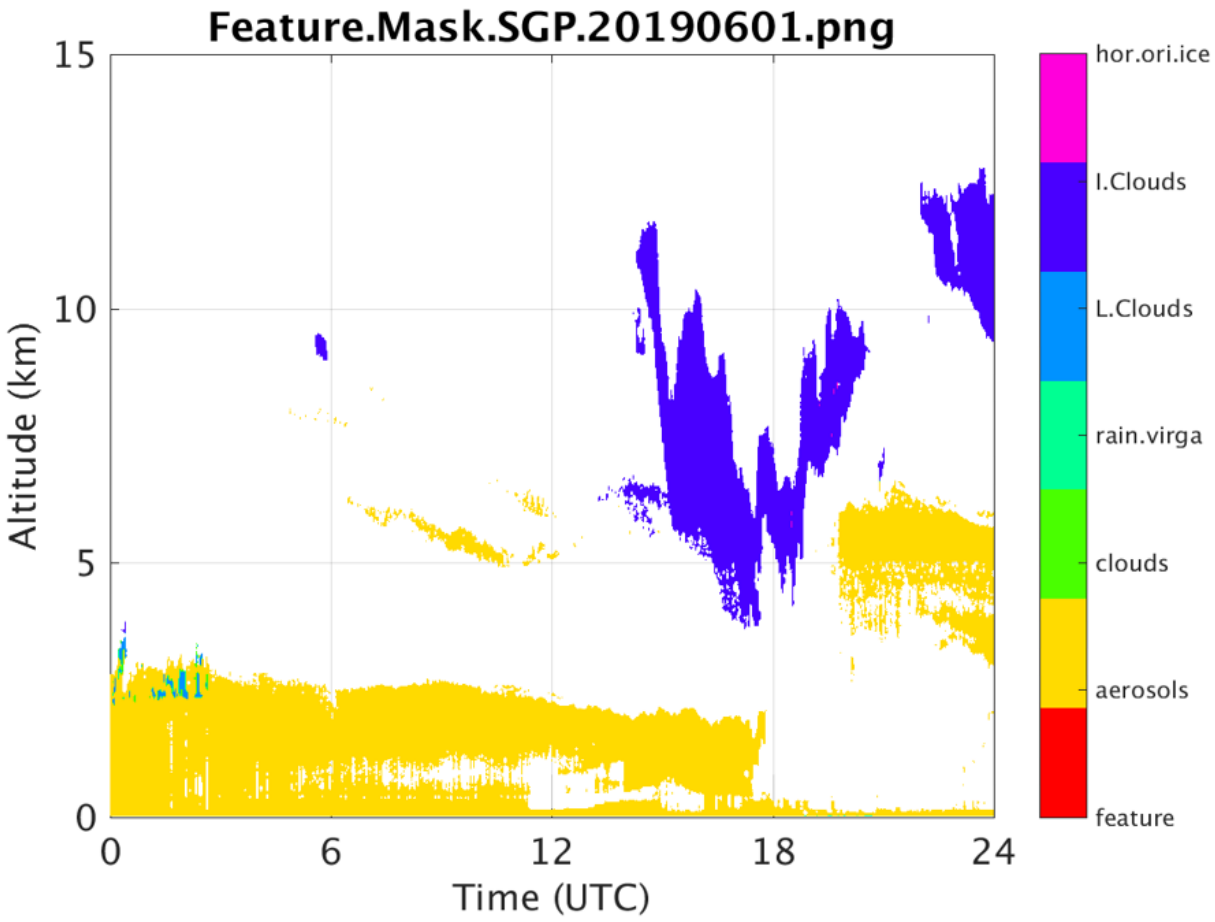

Figure 4. Particulate feature mask from FEX VAP on June 1, 2019 at SGP. The aerosol and cloud features are listed in the vertical color bar. Total confidence score of 0.3 or higher is used in this plot.

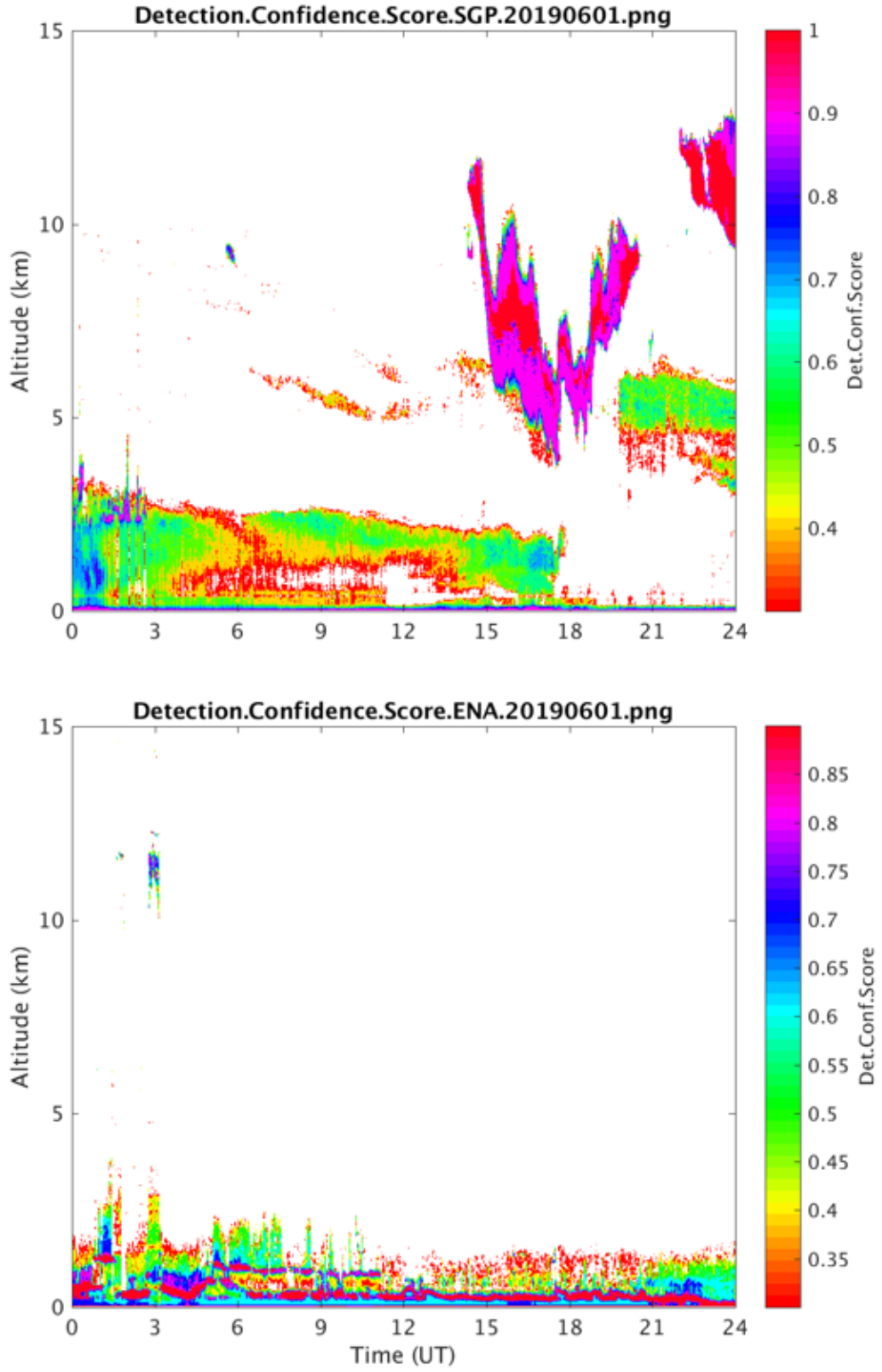

Figure 5. Total detection confidence score with threshold >=0.3 on June 1, 2019 at SGP (top panel) and ENA (bottom panel). In addition to quality flags, total confidence score is one of the key parameters to select good data.

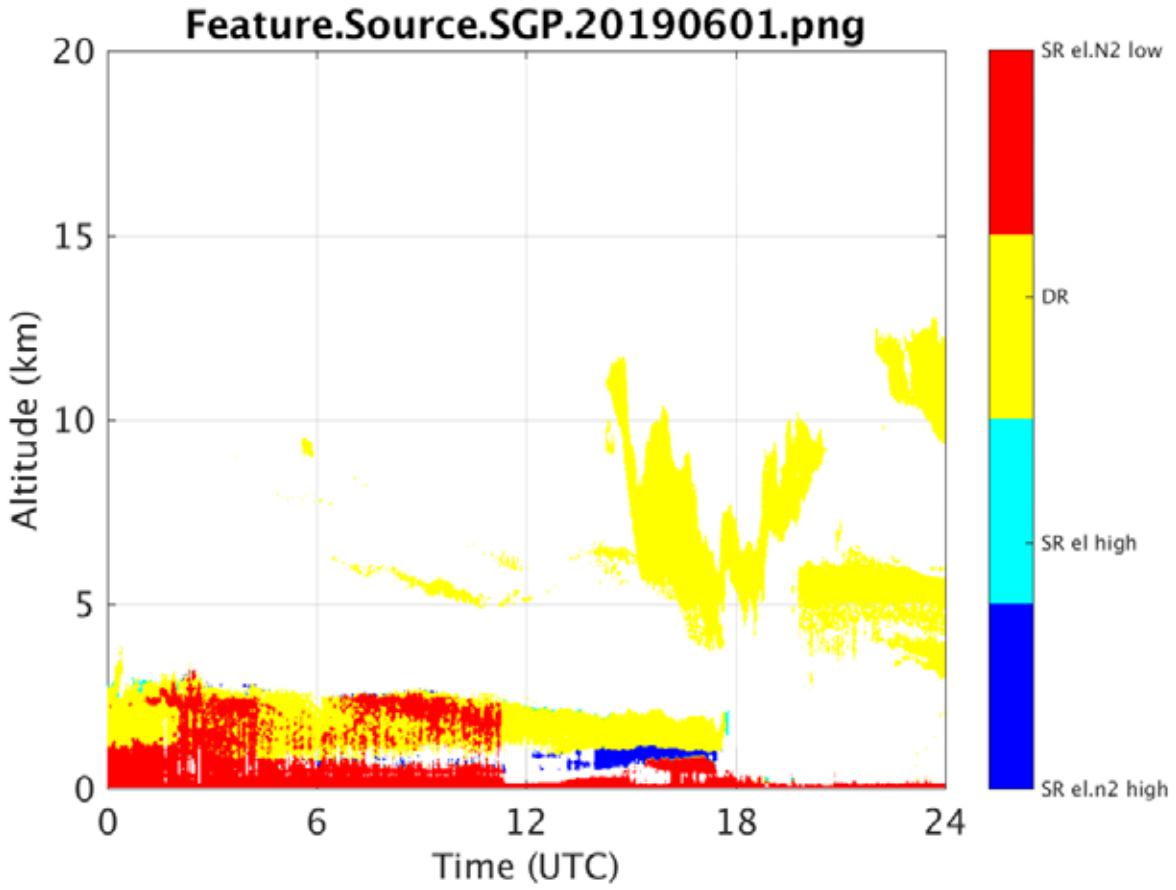

Figure 6. Particulate feature source mask from FEX VAP over SGP on June 1, 2019. Some pixels from multiple features may have overlap. The aerosol and cloud features are listed in the vertical color bar. Total confidence score of 0.3 or higher is used in this plot.

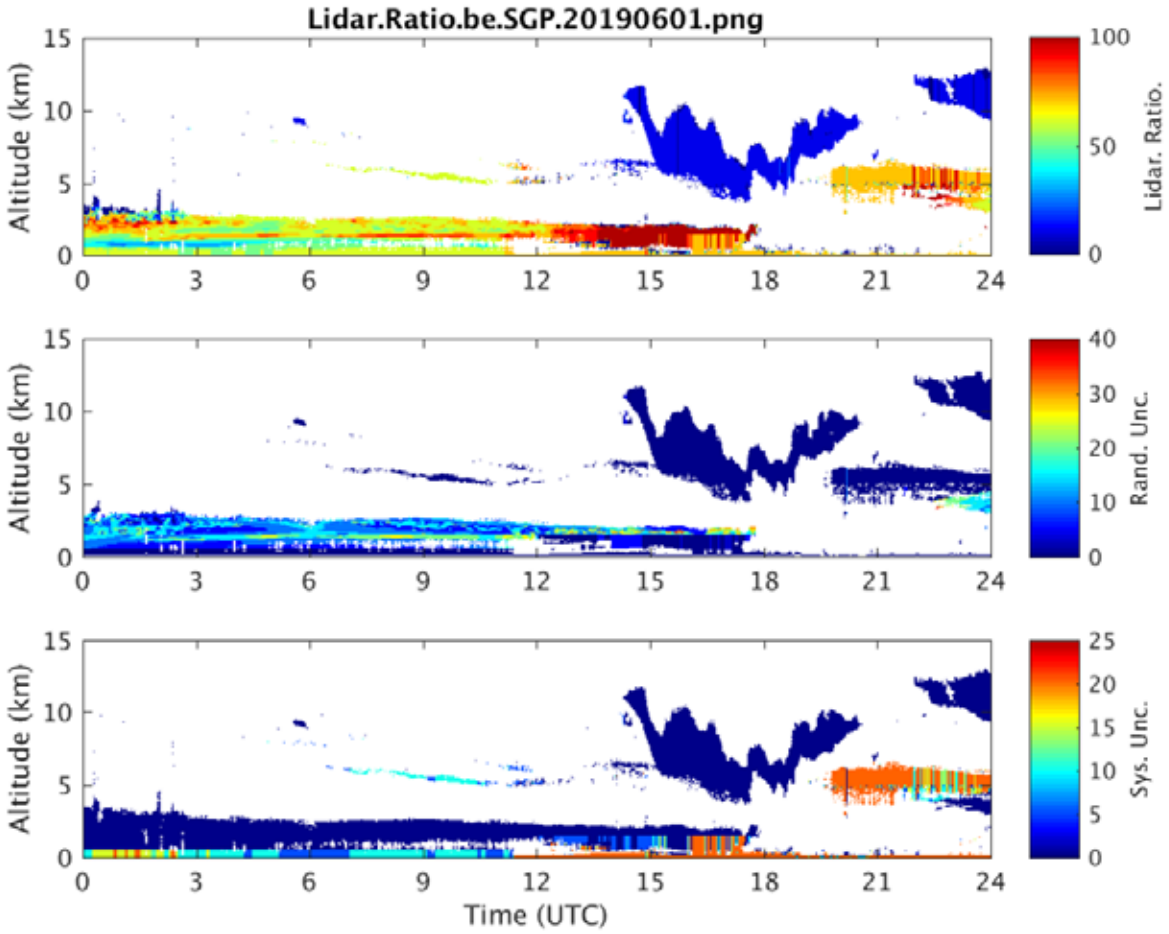

Figure 7. Particulate lidar ratio (top), random (middle), and systematic uncertainties (bottom) panels. Total confidence score of 0.3 or higher is used in this plot.

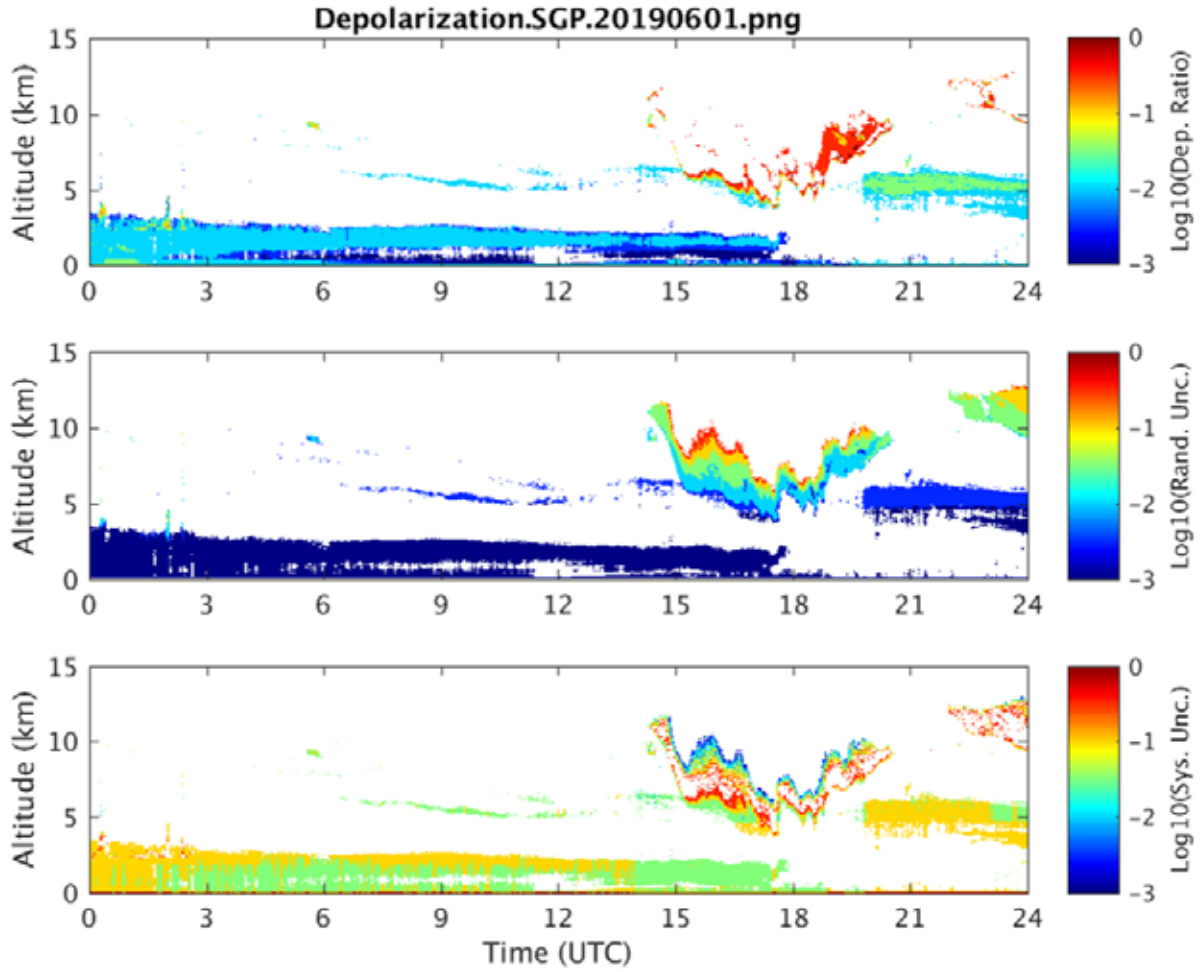

Figure 8. Particulate depolarization (top), random (middle), and systematic uncertainties (bottom) panels for June 1, 2019 at SGP. Total confidence score of 0.3 or higher is used in this plot.

.

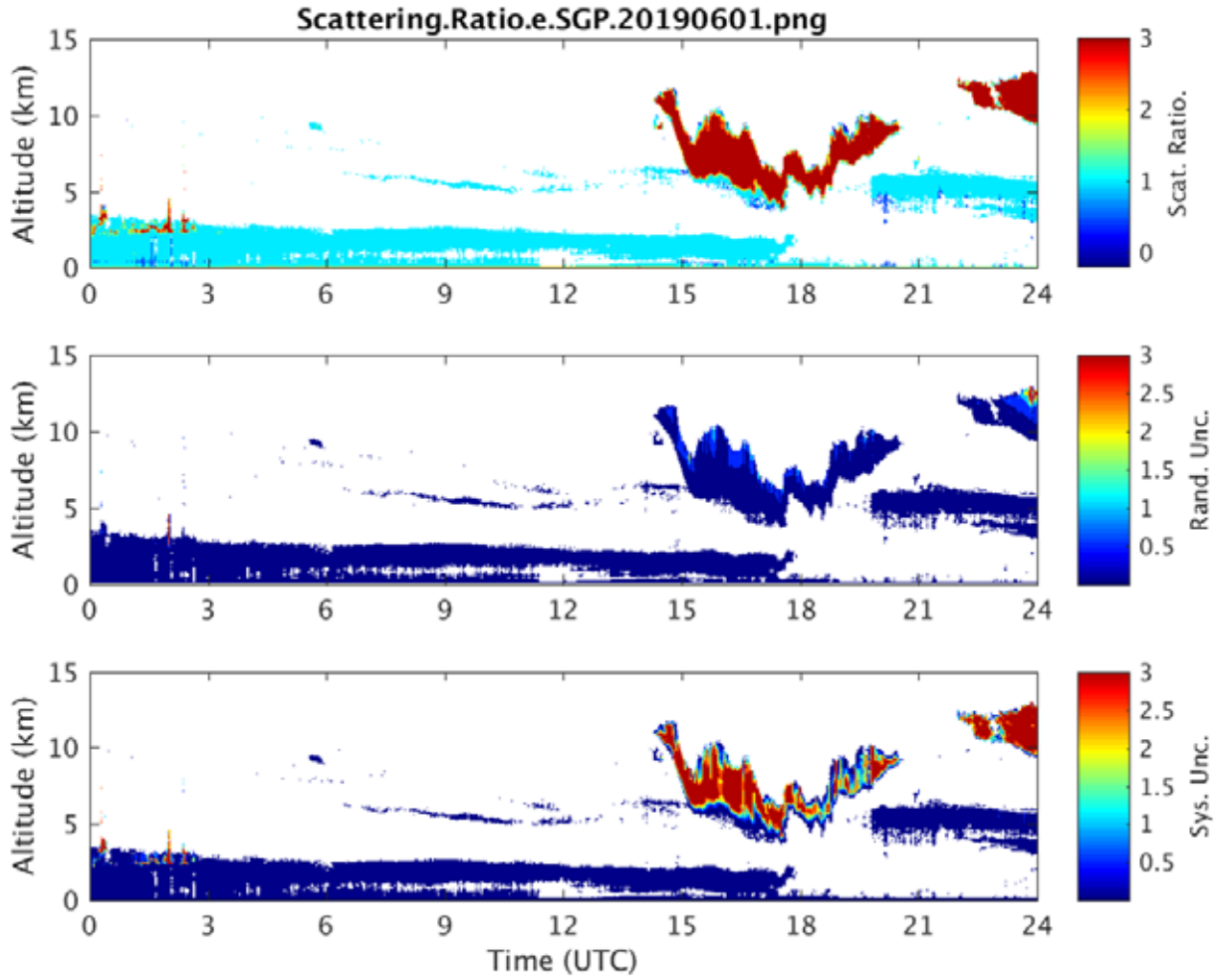

Figure 9. Particulate scattering ratio from elastic signal (top), random (middle), and systematic uncertainties (bottom) panels for June 1, 2019 at SGP. Total confidence score of 0.3 or higher is used in this plot.

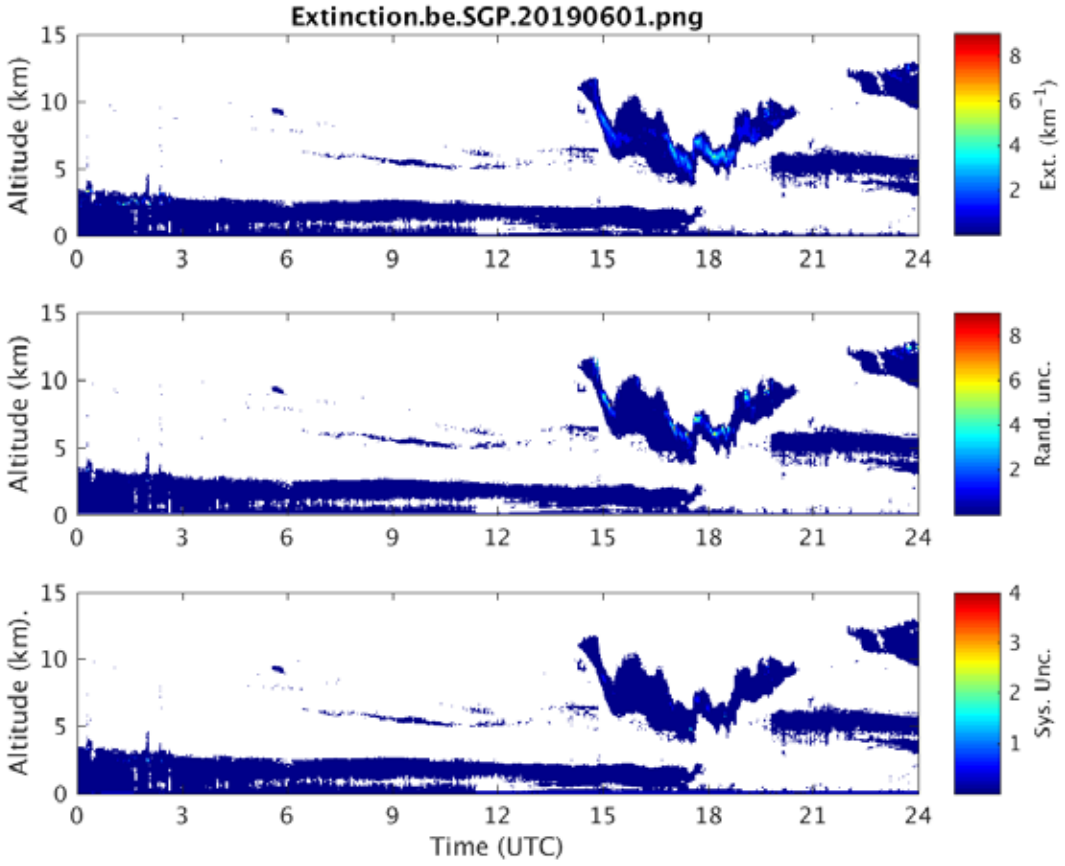

Figure 10. Same as Figure 3 but y axis on linear scale.

8.0 Other Data-Related Information

8.1 Known Algorithm Caveats

In some conditions the VAP yields poor results, e.g., persistent low cloudiness can frustrate accurate calibration. Poor system alignment can reduce sensitivity. Changing alignment can also result in changing calibration that is impossible or difficult to track. Clouds and precipitation can strongly attenuate the beam, resulting in high uncertainty or low confidence scores. The feature mask, total confidence, QC bits, and other related flags can be used to screen the poor-quality data.

8.2 Time Periods Processed

- SGP C1: Available from December 2015 until present.
- ENA C1: Available from November 2015 until present.
- OLI M1: Available from February 2015 to October 2019.

8.3 Data Level/Version Information

One data level (c0) is available from this process. To learn more about the various data levels, please see **here** or go to the link https://www.arm.gov/policies/datapolicies/formatting-and-file-naming-protocols.

8.4 Plans for Future Processing and Modifications

Our next high priority is to apply the FEX algorithm to historical data at SGP C1. Even though the RL has been running for years prior to 2015 at SGP, those data are collected with different system configurations and this VAP can be run for those periods with additional efforts. More resources and efforts are needed to process the historical data.

In a recent study, Balmes et al. (2019) suggested some improvements in the way FEX computes cloud properties. We will assess the impact of these changes and decide if revision is needed in the current FEX VAP.

Since most of the configuration files are made using annual climatology using a couple of years of data, there is room for refining these configuration files using long-term (>10 years) data. There is also room for using seasonal climatology in future.

8.5 Data Tools for ARM netCDF

Output files use the netCDF format, which is standard to all ARM datastreams. The Unidata netCDF home page (https://www.unidata.ucar.edu/software/netcdf/) is the authoritative source for netCDF. A broad variety of tools (freely available and commercial) are accessible through this website and the ARM website https://www.arm.gov/data/work-with-arm-data.

8.6 Frequently Asked Questions

Q: How often does the FEX VAP run?

A: The FEX VAP runs daily at the ARM Data Center (ADC) for SGP C1 and ENA C1.

Q: What kind of data does the FEX VAP provide?

A: The FEX VAP provides best estimates of aerosol extinction and aerosol and cloud features.

Q. What are the inputs to run FEX FAP?

A. It uses lidar raw/merged data, radiosonde data, and configuration files.

Q: Are the FEX VAP products validated by any type of observations?

A: The products are not validated directly with any observations because similar ground-based measurements are not available. The products are compared with limited available observations from satellites. We will intercompare/validate the FEX products when suitable measurements are available.

Q: Does the FEX VAP have outputs from all ARM sites and all times?

A: FEX VAP has been processed from the SGP and ENA sites from 2015 to the present and from the OLI site from 2015 to 2019. The next plan is to process historical data from SGP and tropical sites prior to 2015.

9.0 Contacts

9.1 Instrument Mentor

Name: Rob K. Newsom
Phone: (509) 375-2041
Fax: (509) 372-6020
Mail to: Rob.Newsom@pnnl.gov

9.2 Instrument Translator

Name: Duli Chand
Phone: (509) 375-7241
Fax: (509) 375-6448
Mail to: Duli.Chand@pnnl.gov

9.3 VAP Developers

Erol E. Cromwell
Phone: (509) 372-4648
Fax: (509) 375-3641
Mail to: erol.cromwell@pnnl.gov

Chitra Sivaraman
Phone: (509) 375-2436
Fax: (509) 375-3641
Mail to: Chitra.Sivaraman@pnnl.gov

10.0 References

Balmes, KA, Q Fu, and TJ Thorsen. 2019. “Differences in ice cloud optical depth from CALIPSO and ground-based Raman lidar at the ARM SGP and TWP sites.” *Journal of Geophysical Research – Atmospheres* 124(3): 1755–1778, https://doi.org/10.1029/2018JD028321

Chand, D, R Newsom, J Goldsmith, R Bambha, C Flynn, C Sivaraman, E Cromwell, T Thorsen, and J Comstock. 2019. “Calibration Stability of the ARM Raman Lidar at ENA.” Presented at the ARM/ASR PI science meeting, Washington D.C. https://asr.science.energy.gov/meetings/stm/posters/view?id=2093

Goldsmith JEM, FH Blair, SE Bisson, and DD Turner. 1998. "Turn-key Raman lidar for profiling atmospheric water vapor, clouds and aerosols." *Applied Optics* 37(21): 4979–4990, https://doi.org/10.1364/AO.37.004979

Intergovernmental Panel on Climate Change. 2013. *Climate Change 2013: The Physical Science Basis. Contribution of Working Group I to the Fifth Assessment Report of the Intergovernmental Panel on Climate Change*. Stocker, TF, D Qin, G-K Plattner, M Tignor, SK Allen, J Boschung, A Nauels, Y Xia, V Bex and PM Midgley (eds.). Cambridge University Press, Cambridge, United Kingdom and New York, New York, USA.

Newsom RK. 2009. Raman Lidar Handbook. U.S. Department of Energy. DOE/SC-ARM/TR-038, https://www.arm.gov/publications/tech_reports/handbooks/rl_handbook.pdf

Newsom, RK. 2012. Raman Lidar Profiles Best Estimate Value-Added Products, U.S. Department of Energy. DOE/SC-ARM/TR-100, https://www.arm.gov/publications/tech_reports/doe-sc-arm-tr-100.pdf

Newsom, RK, DD Turner, and JEM Goldsmith. 2013. "Long-term evaluation of temperature profiles measured by an operational Raman lidar." Journal of Atmospheric and Oceanic Technology 30(8): 1616–1634, https://doi.org/10.1175/JTECH-D-12-00138.1

Thorsen, TJ, Q Fu, RK Newsom, DD Turner, and JM Comstock. 2015. "Automated retrieval of cloud and aerosol properties from the ARM Raman lidar. Part I: Feature detection." *Journal of Atmospheric and Oceanic Technology* 32(11): 1977–1998. https://doi.org/10.1175/JTECH-D-14-00150.1

Thorsen, TJ, and Q Fu. 2015. "Automated retrieval of cloud and aerosol properties from the ARM Raman lidar. Part II: Extinction." *Journal of Atmospheric and Oceanic Technology* 32(11): 1999–2023, https://doi.org/10.1175/JTECH- D-14-00178.1

Turner DD, RA Ferrare, LA Heilman Brasseur, WF Feltz, and TP Tooman, 2002. "Automated retrievals of water vapor and aerosol profiles from an operational Raman lidar." *Journal of Atmospheric and Oceanic Technology* 19(1): 37–49, https://doi.org/10.1175/1520-0426(2002)019<0037:AROWVA>2.0.CO;2

Turner, DD, JEM Goldsmith, and RA Ferrare. 2016. *Development and applications of the ARM Raman lidar. The Atmospheric Radiation Measurement Program: The First 20 Years*. Meteorological Monograph 57, American Meteorological Society 18.1-18.15, https://doi.org/10.1175/AMSMONOGRAPHS-D-15-0026.1

Whiteman, DN, B Demoz, P Di Girolamo, J Comer, I Veselovskii, K Evans, Z Wang, M Cadirola, K Rush, G Schwemmer, B Gentry, SH Melfi, B Mielke, D Venable, and T Van Hove. 2006. "Raman Water Vapor Lidar Measurements during the International H_2O Project. I: Instrumentation and Analysis Techniques." *Journal of Atmospheric and Oceanic Technology* 23(2): 157–169, https://doi.org/10.1175/JTECH1838.1

Appendix A

Supplemental Datastreams

A.1 Particulate Backscatter

This datastream has particulate backscatter signals and related information [rlproffexext1thor.c0]. Detailed names of these fields can be taken from the header of each output file by using linux or cygwin terminal command `[ncdump -h filename]` for an individual nc or cdf output file. Also, the detailed list of variable names included in these datastreams can be found at the ARM website: https://engineering.arm.gov/~chand/FEXVAP/. Short and long name of these fields are listed below:

Variable Name	Description
particulate_backscatter_e_n2	Particulate backscatter coefficient calculated from the scattering ratio derived from the high elastic and nitrogen channels
particulate_backscatter_e_n2_uncertainty_random	Random uncertainty in particulate_backscatter_e_n2
particulate_backscatter_e_n2_uncertainty_systematic	Systematic uncertainty in particulate_backscatter_e_n2
particulate_backscatter_e_n2_low	Particulate backscatter coefficient calculated from the scattering ratio derived from the low elastic and nitrogen channels
particulate_backscatter_e_n2_low_uncertainty_random	Random uncertainty in particulate_backscatter_e_n2_low
particulate_backscatter_e_n2_low_uncertainty_systematic	Systematic uncertainty in particulate_backscatter_e_n2_low
particulate_backscatter_e_beS	Particulate backscatter coefficient from the high elastic channels calculated with the Fernald solution using the best-estimate lidar ratios
particulate_backscatter_e_beS_uncertainty_random	Random uncertainty in particulate_backscatter_e_beS
particulate_backscatter_e_beS_uncertainty_systematic	Systematic uncertainty in particulate_backscatter_e_beS
particulate_backscatter_e	Particulate backscatter coefficient from the high elastic channels calculated with the Fernald solution using the high elastic channel lidar ratio
particulate_backscatter_e_uncertainty_random	Random uncertainty in particulate_backscatter_e
particulate_backscatter_e_uncertainty_systematic	Systematic uncertainty in particulate_backscatter_e

Variable Name	Description
lidar_ratio_e_n2	Lidar ratio from the high nitrogen channel extinction and particulate_backscatter_e_n2
lidar_ratio_e_n2_uncertainty_random	Random uncertainty in lidar_ratio_e_n2
lidar_ratio_e_n2_low	Lidar ratio from the low nitrogen channel extinction and particulate_backscatter_e_n2_ low
lidar_ratio_e_n2_low_uncertainty_random	Random uncertainty in lidar_ratio_e_n2_low
lidar_ratio_e	Lidar ratio from the high elastic channels
lidar_ratio_e_uncertainty_random	Random uncertainty in lidar_ratio_e
lidar_ratio_e_uncertainty_systematic	Systematic uncertainty in lidar_ratio_e
source_lidar_ratio_e	Source for field: Lidar ratio from the high elastic channels
particulate_backscatter_be_noMS	Best-estimate of the particulate backscatter coefficient without accounting for multiple scattering effects
lidar_ratio_be_noMS	Best-estimate of the lidar ratio without accounting for multiple scattering effects
particulate_backscatter_e_n2_noMS	Particulate backscatter coefficient calculated from scattering_ratio_e_n2 without accounting for multiple scattering effects
particulate_backscatter_e_n2_low_noMS	Particulate backscatter coefficient calculated from scattering_ratio_e_n2_low without accounting for multiple scattering effects
particulate_backscatter_e_beS_noMS	Particulate backscatter coefficient from the high elastic channels using the best-estimate lidar ratios without accounting for multiple scattering effects
particulate_backscatter_e_noMS	Particulate backscatter coefficient from the high elastic channels without accounting for multiple scattering effects
lidar_ratio_e_n2_noMS	Lidar ratio from the high nitrogen channel extinction and particulate_backscatter_e_n2 without accounting for multiple scattering effects
lidar_ratio_e_n2_low_noMS	Lidar ratio from the low nitrogen channel extinction and particulate_backscatter_e_n2_low without accounting for multiple scattering effects
lidar_ratio_e_noMS	Lidar ratio from the high elastic channels without accounting for multiple scattering effects

A.2 Calibrations

Calibration constants and its related products are listed in this datastream [rlproffexaux1thor.c0]. Detailed names of these fields can be taken from the header of each output file. The short and long names of these fields are listed below:

Variable Name	Description
calibration_e_LH	Low to high elastic channel calibration constant
calibration_e_LH_calc	Low to high elastic channel calibration type
calibration_e_LH_uncertainty_random	Uncertainty in calibration_e_LH
calibration_e_LH_uncertainty_systematic	Uncertainty in calibration_e_LH
calibration_srEN_low	Scattering ratio (low elastic + nitrogen channels) calibration constant
calibration_srEN_low_calc	Low to high elastic + nitrogen channel calibration type
calibration_srEN_low_uncertainty_random	Random uncertainty in calibration_srEN_low
calibration_srEN_low_uncertainty_systematic	Systematic uncertainty in calibration_srEN_low
calibration_srEN	Scattering ratio (elastic + nitrogen channels) calibration constant
calibration_srEN_calc	Scattering_ratio_e_n2 calibration type
calibration_srEN_uncertainty_random	Random uncertainty in calibration_srEN
calibration_srEN_uncertainty_systematic	Systematic uncertainty in calibration_srEN
calibration_srE	Scattering ratio (elastic channel) calibration constant
calibration_srE_calc	Scattering_ratio_e calibration type
calibration_srE_uncertainty_random	Random uncertainty in calibration_srE
calibration_srE_uncertainty_systematic	Systematic uncertainty in calibration_srE
depolarization_misalignment_angle	Misalignment angle between the high parallel and perpendicular channels
depolarization_misalignment_angle_calc	Depolarization misalignment angle calibration type
depolarization_misalignment_angle_uncertainty_random	Random uncertainty in depolarization_misalignment_angle
depolarization_misalignment_angle_uncertainty_systematic	Systematic uncertainty in depolarization_misalignment_angle
overlap_low	Low channels (elastic and nitrogen) overlap function
overlap_low_calc	Function used to calculate low channels overlap function
overlap_low_uncertainty	Uncertainty in overlap_low
overlap_e_high	High elastic channels (parallel and perpendicular channels) overlap function
overlap_e_high_calc	Function used to calculate high elastic channels overlap function
overlap_e_high_uncertainty	Uncertainty in overlap_e_high
overlap_n2_high	High nitrogen channel overlap function
overlap_n2_high_calc	Function used to calculate high nitrogen channels overlap function

Variable Name	Description
overlap_n2_high_uncertainty	Uncertainty in overlap_n2_high
overlap_ratio_e_n2_high	Overlap correction applied to the scattering ratio derived from the high elastic and nitrogen channels
overlap_ratio_e_n2_high_calc	Function used to calculate high elastic to nitrogen channels overlap function
overlap_ratio_e_n2_high_uncertainty	Uncertainty in overlap_ratio_e_n2_high
depolarization_threshold	Threshold used for feature detection in the depolarization ratio
scattering_ratio_e_n2_threshold	Threshold used for feature detection in the scattering ratio derived from high elastic and nitrogen channels
scattering_ratio_e_n2_low_threshold	Threshold used for feature detection in the scattering ratio derived from low elastic and nitrogen channels
scattering_ratio_e_threshold	Threshold used for feature detection in the scattering ratio derived from high elastic channel
multiple_scattering_function_e	Ratio of the total backscatter signal to that from single scattering only in the high elastic channel
qc_multiple_scattering_function_e	Quality check results on field: Ratio of the total backscatter signal to that from single scattering only in the high elastic channel
multiple_scattering_function_n2	Ratio of the total backscatter signal to that from single scattering only in the high nitrogen channel
qc_multiple_scattering_function_n2	Quality check results on field: Ratio of the total backscatter signal to that from single scattering only in the high nitrogen channel
multiple_scattering_function_e_low	Ratio of the total backscatter signal to that from single scattering only in the low elastic channel
qc_multiple_scattering_function_e_low	Quality check results on field: Ratio of the total backscatter signal to that from single scattering only in the low elastic channel
multiple_scattering_function_n2_low	Ratio of the total backscatter signal to that from single scattering only in the low nitrogen channel
qc_multiple_scattering_function_n2_low	Quality check results on field: Ratio of the total backscatter signal to that from single scattering only in the low nitrogen channel
profile_time	Whether it is a day or night time profile
high_parallel_channel_weight	High parallel channel weight
assumed_liquid_cloud_lidar_ratio	Assumed lidar ratio from climatology for liquid cloud
assumed_lce_cloud_lidar_ratio	Assumed lidar ratio from climatology for ice cloud
assumed_horizontal_ice_lidar_ratio	Assumed lidar ratio from climatology for horizontally oriented ice
assumed_aerosol_lidar_ratio	Assumed lidar ratio from climatology for aerosol

Variable Name	Description
assumed_rain_lidar_ratio	Assumed lidar ratio from climatology for rain
assumed_aerosol_angstrom_exponent	Assumed aerosol Angstrom exponent from CIMEL climatology
threshold_coefficient	Threshold coefficient
false_detection_below_height	False detection filter probability below height of complete overlap
false_detection_above_height	False detection filter probability above height of complete overlap
wavelength	Wavelength
attenuation_height	Attenuation height

A.3 System Background

This datastream has background counts and related info [rlproffexcnt1thor.c0]. Detailed names of these fields can be taken from the header of each output file. The short and long names of these fields are listed below:

Variable Name	Description
shots_summed	Number of laser shots in the ensemble
average_energy	Average laser energy of the ensemble shots
background_e_high_para	Background signal in the high elastic parallel channel
background_rms_e_high_para	Background RMS noise in the high elastic parallel channel
background_e_high_perp	Background signal in the high elastic perpendicular channel
background_rms_e_high_perp	Background RMS noise in the high elastic perpendicular channel
background_e_low	Background signal in the low elastic channel
background_rms_e_low	Background RMS noise in the low elastic channel
background_n2_high	Background signal in the high nitrogen channel
background_rms_n2_high	Background RMS noise in the high nitrogen channel
background_n2_low	Background signal in the low nitrogen channel
background_rms_n2_low	Background RMS noise in the low nitrogen channel
counts_e_high_para	Signal in the high elastic parallel channel
counts_e_high_para_uncertainty_random	Random uncertainty in the high elastic parallel channel signal
counts_e_high_para_uncertainty_systematic	Systematic uncertainty in the high elastic parallel channel signal
counts_e_high_perp	Signal in the high elastic perpendicular channel
counts_e_high_perp_uncertainty_random	Random uncertainty in the high elastic perpendicular channel signal
counts_e_high_perp_uncertainty_systematic	Systematic uncertainty in the high elastic perpendicular channel signal

Variable Name	Description
counts_e_low	Signal in the low elastic channel
counts_e_low_uncertainty_random	Random uncertainty in the low elastic channel signal
counts_n2_high	Signal in the high nitrogen channel
counts_n2_high_uncertainty_random	Random uncertainty in the high nitrogen channel signal
counts_n2_low	Signal in the low nitrogen channel
counts_n2_low_uncertainty_random	Random uncertainty in the low nitrogen channel signal
snr_e_high_para	Signal-to-noise ratio in the high elastic parallel channel signal
snr_e_high_perp	Signal-to-noise ratio in the high elastic perpendicular channel signal
qc_snr_e_high	Quality check results on field: Signal-to-noise ratio in the high elastic parallel and perpendicular channel signal
snr_e_low	Signal-to-noise ratio in the low elastic channel signal
qc_snr_e_low	Quality check results on field: Signal-to-noise ratio in the low elastic channel signal
snr_n2_high	Signal-to-noise ratio in the high nitrogen channel signal
qc_snr_n2_high	Quality check results on field: Signal-to-noise ratio in the high nitrogen channel signal
snr_n2_low	Signal-to-noise ratio in the low nitrogen channel signal
qc_snr_n2_low	Quality check results on field: Signal-to-noise ratio in the low nitrogen channel signal

Appendix B

Calibration Stability of the RL System

Operating the lidar systems continuously may change their sensitivities in the long term (days, months, years) due to degrading electronics and optical components. So, in addition to the daily uncertainties, it is important to look at long-term stability of the system. To assure the quality of the Raman lidar (RL) observations and to evaluate the stability of the RL system, we analyzed long-term FEX VAP calibration constants at ARM's ENA site (Chand et al. 2019).

Figure 11 shows the long-term stability of the scattering ratio from the elastic + nitrogen channels. The long-term time series of calibration constants shows a stable and robust system at ENA except one event in the last week of December 2015. This change is due to system update and has no impact on the FEX outcomes.

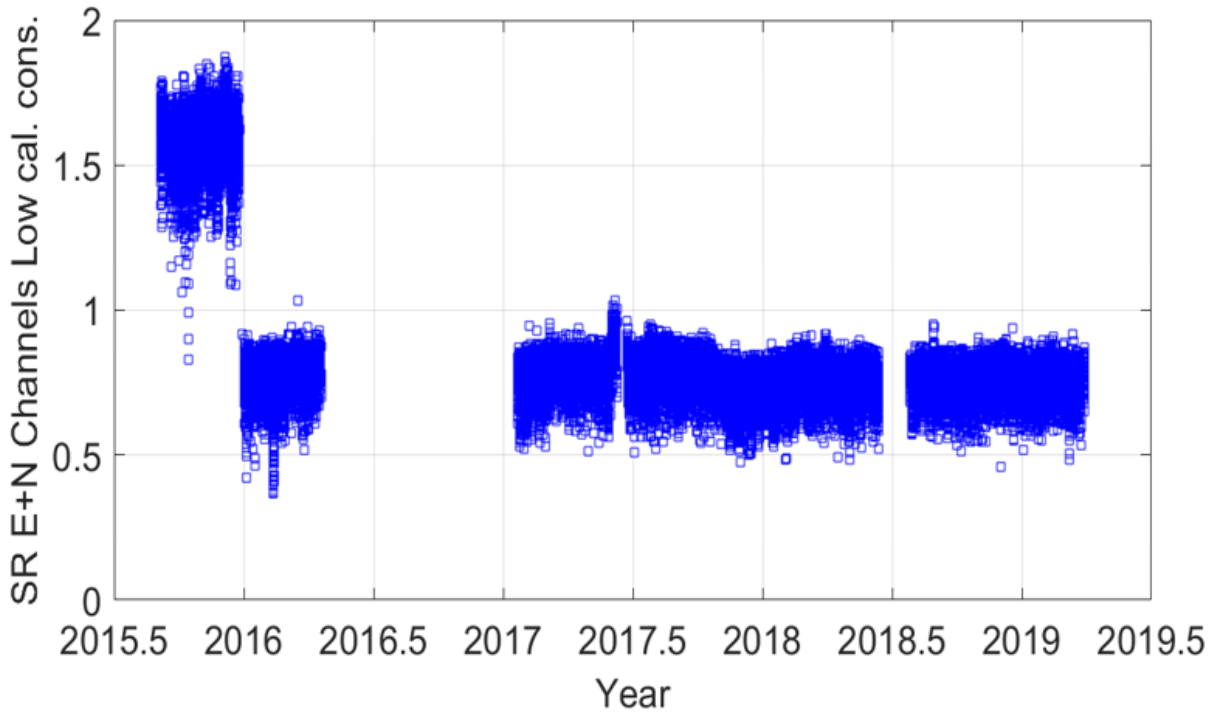

Figure 11. Long-term calibration stability of scattering ratio from elastic + Nitrogen channels. The shift in the last week of 2015 is due to change in the aerosol high and low channels to different voltage supplies as a result of system update. This has no effect on the outcome of FEX VAP.

www.arm.gov